**Rare Metal Materials and Engineering**
Volume 52, Issue 10, October 2023
Available online at www.rmme.ac.cn

Science Press

**Cite this article as**: Kang Jilong, Ma Zhiyao, Li Zhengning, et al. Evolution of $Co_3Sn_2$ Phase Growth Morphology in Undercooled Solidification of Co-Sn Single Phase Alloy[J]. Rare Metal Materials and Engineering, 2023, 52(10): 3410-3416.

ARTICLE

# Evolution of $Co_3Sn_2$ Phase Growth Morphology in Undercooled Solidification of Co-Sn Single Phase Alloy

**Kang Jilong, Ma Zhiyao, Li Zhengning, Chu Ke**

*School of Materials Science and Engineering, Lanzhou Jiao Tong University, Lanzhou 730070, China*

**Abstract:** The undercooled solidification of $(Co_{60}Sn_{40})_{100-x}Nb_x$($x$=0, 0.4, 0.6, 0.8, at% ) single phase alloys was performed to investigate the changes of $Co_3Sn_2$ phase growth morphology. Results show that the $Co_3Sn_2$ phase grows with fractal seaweed morphology at small undercooling ($x$=0, 0.4), and transits to dendrite as the content of added Nb increases to 0.6at%, and then returns to fractal seaweed ($x$=0.8) as a response to the changes in interfacial energy anisotropy and kinetic anisotropy. With the increase in undercooling, the growth morphology of $Co_3Sn_2$ phase in $(Co_{60}Sn_{40})_{99.4}Nb_{0.6}$ alloys returns from dendrite back to factual seaweed at undercooling larger than 28 K and then transits to compact seaweed at undercooling more than 143 K. The minor Nb addition slightly increases the growth velocity of $Co_3Sn_2$ phase at low and intermediate undercooling but obviously decreases the growth velocity at large undercooling. The sharp increase in the growth velocity is corresponding to the transition of $Co_3Sn_2$ phase growth morphology from fractal seaweed to compact seaweed.

**Key words:** undercooled solidification; crystal growth; seaweed; microstructure

Solidification of alloy melts involves the selection of crystal growth pattern, which has a significant effect on the mechanical properties of materials[1–2]. In the directional solidification of Al-4.5wt% Cu alloy, Wang et al[2] found that the ductility and toughness of specimen with a seaweed pattern are approximately 91% and 87% higher than those of specimen with a dendritic pattern, respectively. The interfacial energy and its anisotropy play important roles in governing the morphology of crystal growth from the alloy melts[3–5]. Dendritic microstructures are commonly observed in most alloys due to the large interfacial energy anisotropy[4–6]. Seaweed is another important crystal growth pattern besides dendrite. In the directional solidification of alloy melts, seaweed growth occurs when the preferred crystallographic direction is substantially different from the thermal gradient direction[7–8], and during undercooled solidification, seaweed usually grows at a larger undercooling[9–10]. Recently, it is found that the evolution of microstructure is related to the concentration dependence of interfacial energy anisotropy. In the directional solidification of Al-Zn alloys, Haxhimali et al[11] observed that additions of Zn to Al result in a transition from <100> to <110> growth with increasing Zn concentration, with the seaweed morphology at intermediate compositions. Wang et al[12] studied the solidification behavior of Al-Sm alloys by laser melting, and they also found a similar transition of crystal growth morphology as Sm content increases, and observed the seaweed structure at approximately 2.2at% Sm. Castle et al[13–14] found that minor additions of Ni to Cu melts reduce the undercooling of the Cu melts at which the growth pattern transits from dendritic to seaweed.

Despite aforementioned researches, our understanding about the seaweed growth morphology of crystal in metallic alloy melts is still limited. The Co-Sn alloy is different from most of other binary alloys as it solidifies with a seaweed morphology in undercooling[15–16] and directional solidification[17–18]. In the previous work, the evolution of crystal growth morphology of eutectic and hypereutectic alloy melt was studied, and seaweed growth was observed due to the weak interfacial energy anisotropy of matrix phase $\beta$-$Co_3Sn_2$. According to the Co-Sn binary phase diagram, $Co_3Sn_2$ is an

Received date: February 12, 2023
Foundation item: Gansu Province Science Foundation for Youths (20JR10RA268); Research Fund of Gansu Education Department (2021B-101); Tianyou Youth Talent Lift Program of LZJTU
Corresponding author: Kang Jilong, Ph. D., Associate Professor, School of Materials Science and Engineering, Lanzhou Jiao Tong University, Lanzhou 730070, P. R. China, E-mail: kangjl@lzjtu.edu.cn

intermetallic compound with a slight solid solubility of Co element, so its nominal composition was selected as the concentration of experimental alloy. In the present study, the solidification behavior of the single $Co_3Sn_2$ phase in undercooled $Co_{60}Sn_{40}$ alloys was investigated, and the ternary element Nb was added to further understand the concentration dependence of crystal growth morphology.

## 1 Experiment

In the present study, 0.4at%, 0.6at% and 0.8at% of Nb were added to the base $Co_{60}Sn_{40}$ single phase alloy to investigate the crystal growth morphology evolution. The samples were alloyed from high purity Co (99.99wt%), Sn (99.999wt%) and Nb (99.99wt% ), each about 5 g, and then prepared by induction melting furnace under the protection of high purity argon. In the process of undercooling experiment, the alloy ingot was placed into a quartz glass crucible, and put in a vacuum chamber back-filled with ultrapure argon, then subjected to cyclic induction superheating and cooling under the protection of glass purifier that was made of 50% $B_2O_3$, 30% $Na_2SiO_3$ and 20% $Na_2B_4O_7$ until the desired undercooling was obtained. The thermal history during solidification of each sample was monitored by an infrared pyrometer with a relative accuracy of 1 K and a response time of 1 ms[16] (Fig. 1a). The as-cast samples were used for surface microstructure analysis without any treatment. The surfaces were observed by a scanning electron microscope (SEM) and a Leica optical microscope (OM). The composition of microstructure was measured by energy dispersive X-ray (EDX) analysis. The phase structure analysis of the sample was performed by X-ray diffractometry (XRD) using a scanning step of 4° from $2\theta=20°-80°$. To explore the melting and solidification process, specimens of about 30 mg were cut from the solidified alloy ingots and analyzed in a differential scanning calorimetry (DSC) under a flow of highly-purified argon.

The growth velocity of $Co_3Sn_2$ phase in undercooled $(Co_{60}Sn_{40})_{100-x}Nb_x$ ($x$=0, 0.6) alloys was measured by dual probe method (Fig.1b). Firstly, the cylindrical ingots with a length of 45 mm and a diameter of 7 mm were prepared, and then two probes were placed along the length direction of the ingots with a distance of 30 mm. When the desired undercooling was obtained, trigger nucleation was carried out on the top of the ingots using a $Al_2O_3$ needle. The growth velocity was calculated by dividing the distance difference from the triggering point to the respective viewpoints of the two probes by the time interval for the temperature recalescence front to enter the viewpoint of the two probes (Fig.1b).

## 2 Results and Discussion

### 2.1 Growth behavior of $Co_3Sn_2$ with different Nb additions

During the rapid solidification process of bulk undercooled alloy melts, the crystal grows rapidly, and the latent heat of crystallization is released instantly to form temperature recalescence, which will result in the partial remelting of the primarily solidified phase, so that the initial growth morphology of the primarily solidified phase will be destroyed inside the sample. During the undercooled solidification of some eutectic alloys, such remelting is the main reason for the formation of anomalous eutectic[19]. The surface of the solidified sample is contacted with the cold crucible wall, the latent heat of crystallization can be quickly dissipated to a large extent, the temperature recalescence can be suppressed, and thus a relatively entire morphology of rapidly solidified phase can be maintained to room temperature. Based on the above considerations, the surface rather than the section of the sample was observed by the SEM to investigate the changes of crystal growth morphology under different undercooling conditions. Fig. 2 shows the surface microstructures of $(Co_{60}Sn_{40})_{100-x}Nb_x$ alloy solidified at undercooling of about 5 K.

As shown in Fig. 2a, the primary $Co_3Sn_2$ phase grows with seaweed pattern when the base $Co_{60}Sn_{40}$ is solidified at an undercooling of 5 K. The crystal grows through alternating tip splitting and exhibits no obvious preferences in the growth direction. The two branches after tip splitting have competitive growth with each other. One of the branches outgrows the other and starts to increase its tip radius until it splits again, whereas the other branch decelerates and eventually stops growing. With the addition of 0.4at% Nb, there are some discontinuous straight trunks, and the side branches still present seaweed morphology (Fig. 2b). The microstructure changes to dendrite when the added Nb content increases to 0.6at% to generate the complete main trunks and

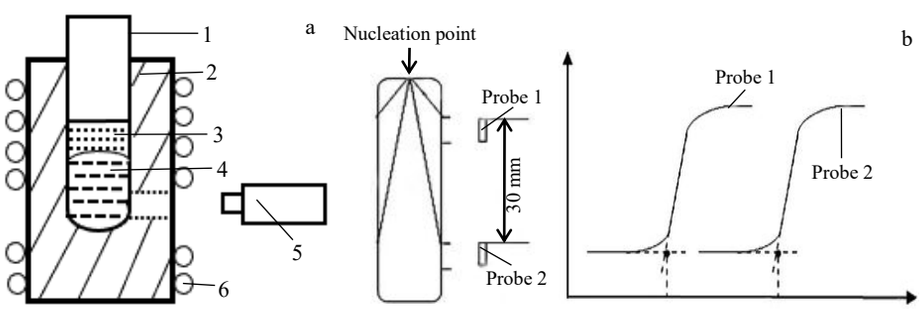


1-quartz glass crucible; 2-refractory base; 3-glass purifier; 4-alloy; 5-infrared pyrometer; 6-induction coil

Fig.1 Schematic diagram of the undercooling experiment (a) and growth velocity measurement by dual probe method (b)

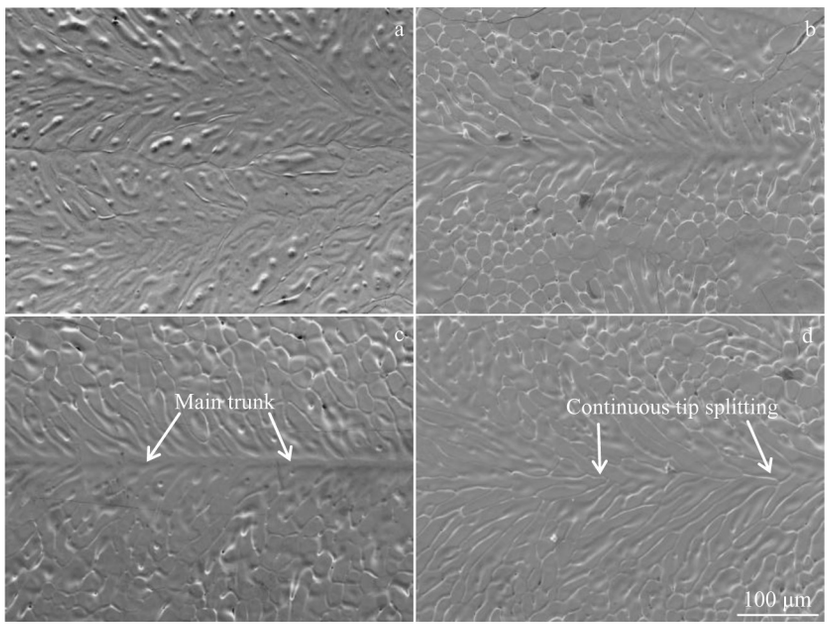


Fig.2 Surface microstructures of $Co_{60}Sn_{40}$ single phase alloy with different Nb additions solidified at an undercooling of about 5 K: (a) 0at%, (b) 0.4at%, (c) 0.6at%, and (d) 0.8at%

abundant side branches have grown from it (Fig. 2c). With further increasing the added Nb content to 0.8at% , the seaweed growth of the $Co_3Sn_2$ phase is observed again (Fig.2d).

Fig. 3 gives XRD patterns of the $(Co_{60}Sn_{40})_{100-x}Nb_x$ alloy. There are two phases identified in all microstructures: $\beta$-$Co_3Sn_2$ and $\alpha$-$Co_3Sn_2$, in which the $\alpha$-$Co_3Sn_2$ is the partial solid-state phase transformation products of $\beta$-$Co_3Sn_2$ during cooling process after solidification. The growth morphology of crystals in the microstructure is mainly determined by $\beta$-$Co_3Sn_2$, and two of them cannot be distinguished in the SEM observation. Fig. 4 shows the results of DSC analysis of $(Co_{60}Sn_{40})_{100-x}Nb_x$ alloys at a heating rate of 20 K/min. The specimens used in the experiment were cut from the master ingots which were solidified under small undercooling, and it is considered to be an equilibrium structure. In DSC curves, there is only one endothermic or exothermic peak on the heating and cooling curve, so it is considered to be a single

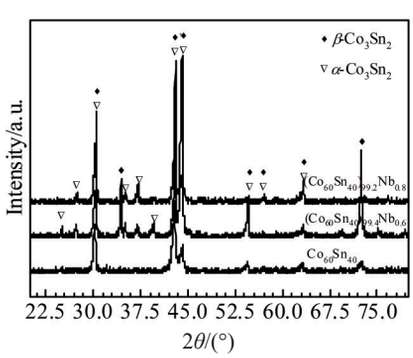


Fig.3 XRD patterns of $(Co_{60}Sn_{40})_{100-x}Nb_x$ alloy

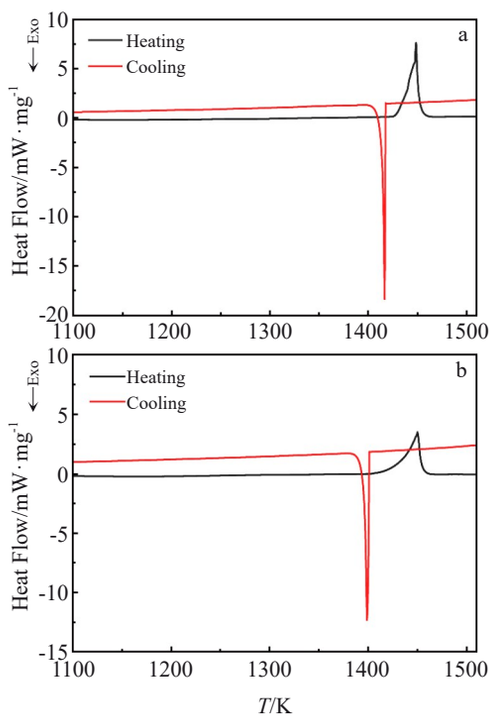


Fig.4 DSC curves of $Co_{60}Sn_{40}$ (a) and $(Co_{60}Sn_{40})_{99.2}Nb_{0.8}$ (b) alloys at a heating rate of 20 K/min

phase alloy. The addition of Nb does not result in the formation of new phase, and only changes the growth behavior of $Co_3Sn_2$ phase.

The strength of interfacial energy anisotropy is an important factor affecting the crystal growth morphology during solidification. In undercooled solidification, the stronger interfacial energy anisotropy will lead to dendritic growth of

crystal. Instead, the crystal adopts a seaweed morphology. However, it is difficult to directly measure the interfacial energy anisotropy in experiments, so we calculated the surface energy of $Co_3Sn_2$ phase and its anisotropy parameter according to the empirical electron theory of solids and molecules[20] in the present study. As for hcp structure, the surface energy of a particular (*hkil*) crystallographic plane relative to the close-packed basal plane (0001) can be expressed as:

$$\frac{\gamma_{(hkil)}}{\gamma_{(0001)}}=\frac{Aa}{c}\sum_{\alpha}^{(hkil)}I_\alpha E_\alpha \Big/ \sum_{\alpha}^{(0001)}I_\alpha E_\alpha \quad (1)$$

where $A$ is a constant related to the crystal plane, $a$ and $c$ are the lattice constants, $I_\alpha$ is the number of equivalent dangling bonds on the given crystal plane, and $E_\alpha$ is the bond energy between the atoms. The anisotropy strength between (*hkil*) plane and the (0001) basal plane is:

$$\varepsilon=\frac{\gamma_{(hkil)}-\gamma_{(0001)}}{2\gamma_0} \quad (2)$$

where $\gamma_0$ is the average value of $\gamma_{(hkil)}$ and $\gamma_{(0001)}$.

The calculated maximum anisotropy strength of hexagonal $Co_3Sn_2$ phase is between $(10\bar{1}0)$ plane and (0001) plane, and the value is only 0.204. Compared to the surface energy anisotropy of other metals, the value is 0.252 for Al phase[21] and 0.376 for Zn[22] phase whose solids grow with dendritic morphology in their alloy melts. Hence, the hexagonal $Co_3Sn_2$ phase has relatively low interfacial energy anisotropy, so that the crystal should grows with seaweed morphology in the undercooled solidification of Co-Sn alloys[3,5], as shown in Fig.2a.

Because the mixing enthalpy of Nb-Co and Nb-Sn is −25 and − 1 kJ/mol, respectively, the value of Nb-Co is more negative than Nb-Sn[23], in the undercooled solidification of $(Co_{60}Sn_{40})_{100-x}Nb_x$ alloy melts, and the added Nb atoms are incorporated into the solid $Co_3Sn_2$ phase to form $Co_3(Sn,Nb)_2$. However, the atomic radius of Sn is 0.162 nm, 0.143 nm larger than the atomic radius of Nb, indicating that the $Co_3Sn_2$ lattice will shrink as Nb substitute for Sn, and resulting in the decrease in the *c*/*a* ratio. According to Eq. (1) and Eq. (2), it can be obtained that the surface energy ratio between (*hkil*) and (0001) for $Co_3(Sn,Nb)_2$ is larger than that for $Co_3Sn_2$. The surface energy anisotropy of $Co_3Sn_2$ phase increases with the addition of Nb, so the growth morphology of $Co_3Sn_2$ transits to dendrite with the addition of 0.6at% Nb (Fig.2c).

With the addition of Nb to $Co_{60}Sn_{40}$ alloy, the concentration of Nb in the solid $Co_3Sn_2$ also increases. The entropy of this phase rises. On the basis of DSC analysis (Fig. 4), when 0.8at% Nb is added, the enthalpy of fusion of $Co_3Sn_2$ decreases from 95325 J/mol to 79845 J/mol. Therefore, the entropy of fusion of $Co_3Sn_2$ decreases, which will cause a rough solid/liquid interface, and thus weakens the atomic attachment kinetic anisotropy[24]. This will partially offset the stabilization effect of the interfacial energy anisotropy on the branching tip. As a result, the growth morphology of $Co_3Sn_2$ phase returns back to the seaweed pattern in the $(Co_{60}Sn_{40})_{99.2}Nb_{0.8}$ alloy. This experimental result is qualitatively consistent with the findings of Castle et al[13–14] about the undercooled solidification of Cu-Ni alloys. They found that with the increase in solute content, the critical undercooling for the crystal growth morphology changes from dendrite to seaweed decreases. In this respect, the Nb content in the alloy melts increases slightly from 0.6at% to 0.8at% , which is conducive to the seaweed growth.

### 2.2 Growth velocity of $Co_3Sn_2$ phase

Fig.5 gives the growth velocity of $Co_3Sn_2$ phase in $Co_{60}Sn_{40}$ and $(Co_{60}Sn_{40})_{99.4}Nb_{0.6}$ alloys under various undercooling conditions. In the range of experimental undercooling, the growth velocity ($V$) of $Co_3Sn_2$ phases increases with undercooling ($\Delta T$). A power law trend is fitted to the data sets and expressed as: $V \propto \Delta T^e$, where $e$ is the exponent of undercooling. As for $Co_{60}Sn_{40}$ and $(Co_{60}Sn_{40})_{99.4}Nb_{0.6}$ alloys, the crystal growth velocity increases slowly up to 129 and 143 K undercooling, with the exponent of 2.14 and 1.71, respectively, and then increases rapidly, thereafter a breakdown in this trend is observed. The values of exponent increase to 5.31 and 5.74. This change of $Co_3Sn_2$ phase growth velocity under the critical undercooling corresponds to its growth morphology transition from fractal to compact seaweed, as shown in Fig. 6 and Fig. 7. On closer inspection, the addition of 0.6at% Nb to $Co_{60}Sn_{40}$ alloy results in an increase in the growth velocity of $Co_3Sn_2$ phases when the solidified undercooling is less than 116 K, but the growth velocity decreases at higher undercooling.

The redistribution coefficient of Nb in the $Co_3Sn_2$ phase is 0.44, less than unity[15]. Therefore, in undercooled solidification, Nb atoms will be rejected by the growing $Co_3Sn_2$ phase and pile up ahead of the solid/liquid interface to form a constitutional undercooling zone, which slows down the growth velocity of $Co_3Sn_2$ phase when the undercooling is larger than 116 K. However, a small amount of Nb will make the growing tip of $Co_3Sn_2$ phase decrease to dissipate the enriched Nb efficiently. As a result, the growth of $Co_3Sn_2$ phase in $(Co_{60}Sn_{40})_{99.4}Nb_{0.6}$ alloys should be accelerated at the undercooling less than 116 K because the effect on sharpening the tip radius of $Co_3Sn_2$ by the minor Nb addition is more

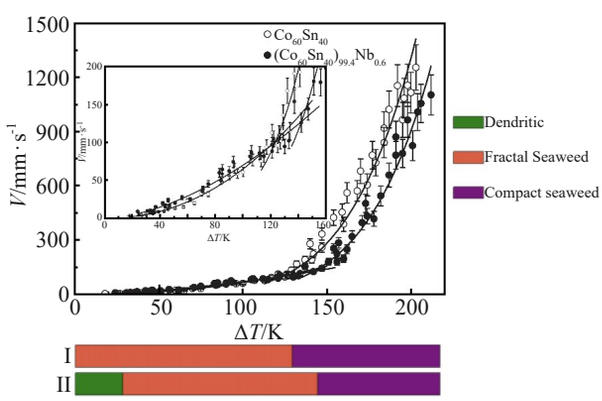


Fig.5 Measured crystal growth velocity of $Co_3Sn_2$ phase with undercooling in rapid solidification of $(Co_{60}Sn_{40})_{100-x}Nb_x$ alloy

significant, as shown in Fig. 5. This effect of a small amount solute element on crystal growth velocity is common in the solidification of pure metals[25]. During the crystal growth of single $Co_3Sn_2$ phase in $Co_{60}Sn_{40}$ alloy melts, a few solute atoms will be rejected by growing solid, and there is no mutual diffusion of atoms in eutectic growth, so the crystal growth velocity is larger than that of the hypereutectic and eutectic alloys[15].

### 2.3 Morphology evolution of $Co_3Sn_2$ phase with undercooling

Fig. 6 shows the SEM surface microstructures of the base $Co_{60}Sn_{40}$ alloy samples after solidification at different undercooling. The $Co_3Sn_2$ phase grows with seaweed morphology under all experimental undercooling conditions, but its characteristic scale is related to solidification undercooling. The calculated fractal dimensions of the structures by the box counting method[5] are about 1.70 when the solidification undercooling is below 129 K, meaning that the growth microstructure is fractal seaweed (Fig. 6a and 6b). While the calculated fractal dimension of the microstructures solidified at a larger undercooling is very near to 2, indicating that the growth morphology of the $Co_3Sn_2$ phase changes to compact seaweed pattern. In the compact growth of $Co_3Sn_2$ phase, the two branches after tip-splitting grow relatively independently, the branch becomes very short, which are symmetrically distributed behind the tips (Fig. 6c and 6d), and result in a dense structure.

Fig. 7 gives the surface microstructures of the $(Co_{60}Sn_{40})_{99.4}Nb_{0.6}$ alloy melts solidified at different undercooling. When the alloy melts are solidified at a small undercooling, the $Co_3Sn_2$ phase grows with dendritic pattern and features straight dendrite arms, and the secondary, or even the tertiary arms, outgrow from the trunk (Fig. 7a). When the undercooling is larger than 28 K, the crystal grows with continuous alternating tip splitting, so the growth morphology of $Co_3Sn_2$ phase changes to the fractal seaweed (Fig. 7b and 7c). As the undercooling increases to more than 143 K, the $Co_3Sn_2$ phase grows with the compact seaweed (Fig. 7d and 7e). Therefore, the addition of 0.6at% Nb to $Co_{60}Sn_{40}$ alloy results in an increase in the critical undercooling for the $Co_3Sn_2$ phase growth morphology transition from fractal to compact seaweed.

The effect of undercooling on the growth morphology of $Co_3Sn_2$ phase is related to crystal growth kinetics. The crystal growth velocity is faster with the increase in undercooling, as shown in Fig. 5. The atoms in the liquid phase deposit to the solid phase in a freer manner, resulting in a rougher solid/liquid interface in atomic-level at large undercooling.

Hence, the effect of interfacial energy anisotropy on branching the interface is partially offset, and the effective dynamic anisotropy in undercooled solidification is weakened[24], which promotes the formation of fractal seaweed at the undercooling larger than 28 K for $(Co_{60}Sn_{40})_{99.4}Nb_{0.6}$ alloy. In addition, to adapt to the increase in crystal growth velocity with undercooling, there is a decrease in the interface tip radius, so the corresponding possibility for the tip splitting will decrease. What's more, the perturbations that initially branches the interface will leave the tip region more quickly at large growth velocity, which facilitates the stabilization of the interface tip also. Therefore, it tends to branch deviating from the exact tip, and forms side branch. Hence the growth morphology of $Co_3Sn_2$ phase transits from fractal seaweed to compact seaweed above the undercooling of 129 K in $Co_{60}Sn_{40}$ alloy. The added 0.6at% Nb to $Co_{60}Sn_{40}$ alloy decreases the growth velocity of $Co_3Sn_2$ at a large undercooling, as shown in Fig. 5, so the critical undercooling of crystal growth morphology transformation will be increased to 143 K in $(Co_{60}Sn_{40})_{99.4}Nb_{0.6}$ alloy.

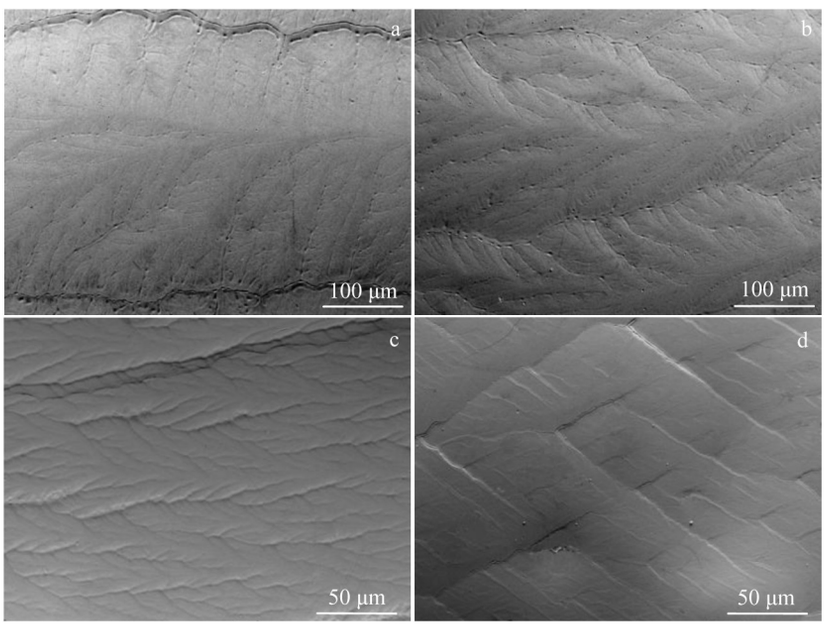


Fig.6 SEM surface micrographs of the $Co_{60}Sn_{40}$ alloys solidified at different undercooling: (a) 25 K, (b) 122 K, (c) 129 K, and (d) 213 K

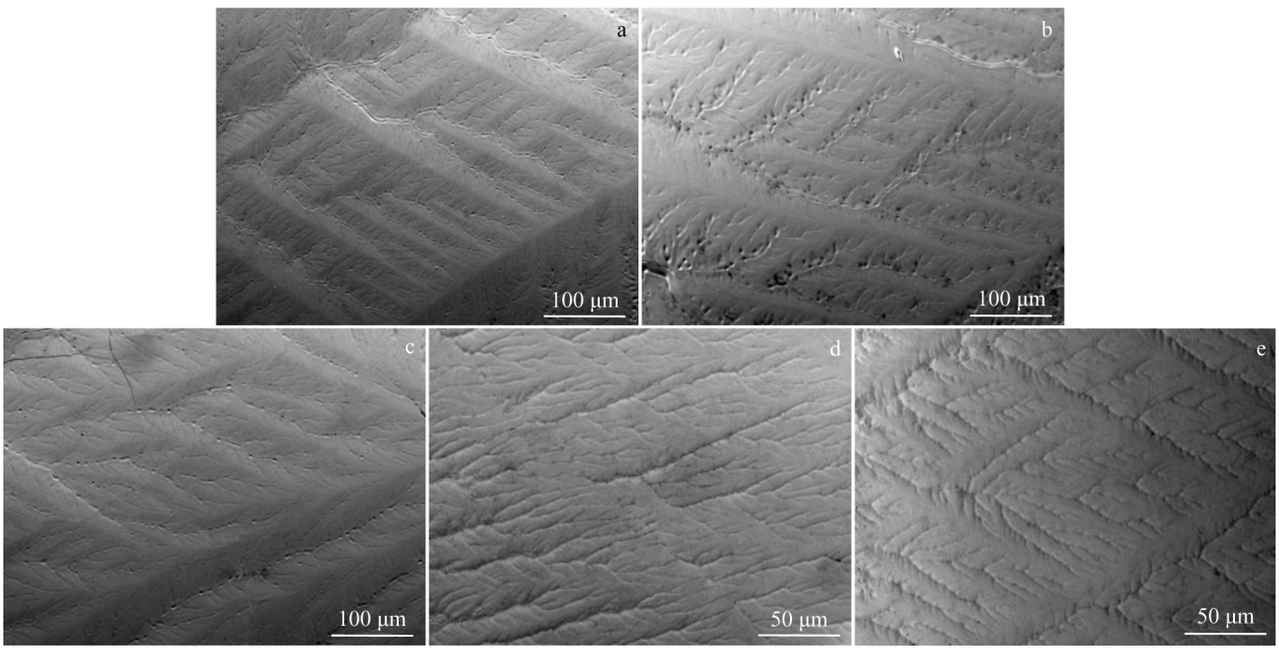


Fig.7 SEM surface micrographs of $(Co_{60}Sn_{40})_{99.4}Nb_{0.6}$ alloy solidified at different undercooling: (a) 23 K, (b) 28 K, (c) 138 K, (d) 143 K, and (e) 207 K

## 3 Conclusions

1) When Nb content is 0.6at% , the seaweed growth morphology of $Co_3Sn_2$ phase changes to dendritic morphology, and returns back to seaweed with an addition of 0.8at% Nb. The addition of Nb enhances the interfacial energy anisotropy and weakens the kinetic anisotropy, resulting in the changes of growth morphology.

2) In undercooled solidification of $(Co_{60}Sn_{40})_{99.4}Nb_{0.6}$ alloys, with the increase in undercooling, the growth morphology of $Co_3Sn_2$ phase successively transits from dendrite, factual seaweed then to compact seaweed. Compared to $Co_{60}Sn_{40}$ alloy, the added 0.6at% Nb increases the critical undercooling for the $Co_3Sn_2$ phase transformation from fractal to compact seaweed.

3) The addition of 0.6at% Nb to $Co_{60}Sn_{40}$ alloy results in an increase in the growth velocity of $Co_3Sn_2$ phases when the solidified undercooling is less than 116 K, but the growth velocity obviously decreases at larger undercooling. The sharp increase in the growth velocity is corresponding to the transition of $Co_3Sn_2$ phase growth morphology from fractal seaweed to compact seaweed.

## References

1 Pu D M, Chen X H, Ye J L *et al*. *Rare Metal Materials and Engineering*[J], 2022, 51(12): 4436

2 Wang Y M, Li S M, Yang B *et al. Materials Science & Engineering A*[J], 2020, 771: 138 665

3 Brener E, Muller-Krumbhaar H, Temkin D. *Physical Review E*[J],1996, 52: 2714

4 Strickland J, Nenchev B, Dong H. *Crystals*[J], 2020, 10: 627

5 Ihle T, Müller Krumbhaar H. *Physical Review E*[J], 1994, 49: 2972

6 Provatas N, Wang Q, Haataja M *et al. Physical Review Letters*[J], 2003, 91: 155 502

7 Xing H, Ji M Y, Dong X L *et al. Materials and Design*[J], 2020, 185: 108 250

8 Pocheau A, Deschamps J, Georgelin M. *Journal of the Minerals Metals & Materials society*[J], 2007, 59: 71

9 Haque N, Cochrane R F, Mullis A M. *Intermetallics*[J], 2016, 76: 70

10 Jiang A, Wang X. *Acta Materialia*[J], 2020, 200: 56

11 Haxhimali T, Karma A, Gonzales F *et al. Nature Materials*[J], 2006, 5: 660

12 Wang L, Hoyt J J, Wang N *et al. Nature Communications*[J], 2020, 11: 724

13 Castle E G, Mullis A M, Cochrane R F. *Acta Materialia*[J], 2014, 66: 378

14 Castle E G, Mullis A M, Cochrane R F. *Acta Materialia*[J], 2014, 77: 76

15 Kang J L, Li J F, Wei X X *et al. Metallurgical and Materials Transactions A*[J], 2016, 47: 6187

16 Liu L, Li J F, Zhou Y H. *Acta Materialia*[J], 2011, 59: 5558

17 Kang J L, Li J F. *Metallurgical and Materials Transactions A*[J], 2020, 51: 6346

18 Kang J L, Zhao M. *Materials Science and Technology*[J], 2022, 38: 191

19 Liu L J, Wei X X, Ferry M *et al. Scripta Materialia*[J], 2020, 174: 72

20 Guo Y Q, Yu R H, Zhang R L *et al. Journal of Physical Chemistry B*[J], 1998, 102: 9

21 Zhang J M, Ma F, Xu K W. *Applied Surface Science*[J], 2004, 229: 34
22 Fu B Q, Liu W, Li Z L. *Applied Surface Science*[J], 2009, 255: 9348
23 Senkov O N, Miracle D B. *Materials Research Bulletin*[J], 2001, 36: 2183
24 Assadi H, Oghabi M, Herlach D M. *Acta Materialia*[J], 2009, 57: 1639
25 Karma A, Langer J S. *Physical Review A*[J], 1984, 30: 3147

# Co-Sn单相合金深过冷凝固时$Co_3Sn_2$相生长形貌的演变机制

康纪龙，马志尧，李正宁，褚　克
(兰州交通大学 材料科学与工程学院，甘肃 兰州 730070)

**摘　要：**开展了$(Co_{60}Sn_{40})_{100-x}Nb_x$($x$=0，0.4，0.6，0.8，at%)单相合金的深过冷凝固实验，研究了$Co_3Sn_2$相生长形貌的演变机制。结果表明，在小过冷度下，$Co_3Sn_2$相在$x$=0，0.4以海藻状的模式进行生长，随着添加的Nb含量增加至0.6at%，其生长形貌转变为树枝晶，并在$x$=0.8进一步转变为分形海藻晶，这主要是由于界面能各向异性和动力学各向异性的变化。随着过冷度的增加，$(Co_{60}Sn_{40})_{99.4}Nb_{0.6}$合金中$Co_3Sn_2$相生长形貌在过冷度大于28 K时从树枝晶转变为分形海藻，当过冷度高于143 K时转变为密集海藻。少量的Nb添加在小过冷度和中间过冷度时能提高$Co_3Sn_2$相的生长速度，但是在大过冷度下会显著降低生长速度。$Co_3Sn_2$相生长速度随过冷度变化规律的转变对应其生长形貌从分形海藻向密集海藻的转变。

**关键词：**过冷凝固；晶体生长；海藻晶；微观组织

---

作者简介：康纪龙，男，1988年生，博士，副教授，兰州交通大学材料科学与工程学院，甘肃 兰州 730070，E-mail：kangjl@lzjtu.edu.cn